Eur. Phys. J. A (2022) 58:57
https://doi.org/10.1140/epja/s10050-022-00711-z

THE EUROPEAN PHYSICAL JOURNAL A

Special Article - New Tools and Techniques

Commissioning of the 4π γ-summing array HECTOR at CASPAR: measurements of ^{27}Al$(p,\gamma)^{28}$Si resonances 4850 feet underground

O. Olivas-Gomez[1,a], A. Simon[1,b], D. Robertson[1], A. C. Dombos[1], F. Strieder[2], T. Kadlecek[2], M. Hanhardt[2,3], R. Kelmar[1], M. Couder[1], J. Görres[1], E. Stech[1], M. Wiescher[1]

[1] Department of Physics and Joint Institute for Nuclear Astrophysics, University of Notre Dame, Notre Dame, IN 46556, USA
[2] Department of Physics, South Dakota School of Mines and Technology, Rapid City, SD 57701, USA
[3] South Dakota Science and Technology Authority, Sanford Underground Research Facility, Lead, SD 57754, USA

Received: 10 August 2021 / Accepted: 20 March 2022 / Published online: 31 March 2022

Communicated by Anu Kankainen

Abstract The High EffiCiency TOtal absorption spectrometeR (HECTOR) is a 4π γ-summing detector designed to measure capture cross sections. Here, we present the commissioning of HECTOR at the Compact Accelerator System for Performing Astrophysical Research (CASPAR) laboratory, which is located at the Sandford Underground Research Facility 4850 feet underground. With the underground environment drastically improving the signal-to-noise ratio of the detector, it is estimated HECTOR will be able to push cross-section measurements below a nanobarn. Details of the experimental setup are discussed along with the analysis of several resonance strengths measured for the ^{27}Al$(p,\gamma)^{28}$Si reaction between the lab energies 0.2–1.0 MeV. The measurements are in excellent agreement with those found in the literature.

1 Introduction

To better our understanding of stellar nucleosynthesis, there is a drive to experimentally measure nuclear reaction cross sections important to stellar burning processes over the astrophysically relevant energy ranges. Of particular interest are reactions thought to be sources of neutrons for the s-process, one of the primary mechanisms for creating the elements above the iron peak [1]. This includes (α, n) reactions producing these neutrons as well as the competing (α, γ) reactions. However, the astrophysical energy ranges for these reactions occur on the order of hundreds of keV where the cross section exponentially drops due to the Coulomb barrier.

In order to measure the rapidly declining cross sections in this energy region, a highly efficient detector setup with a good signal-to-noise ratio is desirable. This can be achieved using deep underground research facilities (e.g., [2–5]) which provide shielding from cosmic-muon rays. Here we present the setup of High EffiCiency TOtal absorption spectrometeR (HECTOR) at the Compact Accelerator System for Performing Astrophysical Research (CASPAR) laboratory [5]. The laboratory is located 4850 feet underground within the Sanford Underground Research Facility in South Dakota, United States.

HECTOR is a 4π γ-summing detector comprised of 16 segments. Each segment contains a $4'' \times 8'' \times 8''$ NaI(Tl) crystal enclosed by a 1-mm thick aluminum casing. The crystals were manufactured by Saint-Gobain Crystals [6]. Scintillation light from each crystal is read out by two 3" diameter 10-stage photomultiplier tubes (PMT). A 60 mm bore hole through the detector allows for placing of the target in the center of the array without compromising the solid angle covered by the detector.

HECTOR was first commissioned at the Nuclear Science Laboratory (NSL) at the University of Notre Dame [7] and has since been used to measure several (α, γ) and (p, γ) reactions related to explosive nucleosynthesis [8,9]. HECTOR operates on the principle of the γ-summing technique, a well-established method for cross-section measurements [10]. After a particle capture, the residual nucleus is formed in an excited state with energy $E_\Sigma = E_{cm} + Q$, where E_{cm} is the energy in the center of mass frame and Q is the Q value of the reaction. It then promptly decays with the release of one or several γ rays as it transitions towards the ground state. Instead of analyzing each individual γ ray, HECTOR is able to simultaneously detect and sum the energies of all

[a] e-mail: ogomez@nd.edu (corresponding author)
[b] e-mail: anna.simon@nd.edu

emitted γ rays, forming a single peak known as the sum peak at E_Σ. The yield of the reaction —which is proportional to the total-reaction cross section— is then given by the number of counts in the sum peak corrected by a summing efficiency. The summing efficiency takes into account the efficiency of the detector due to each γ ray from all the cascades transitioning to the ground state. The summing efficiency is discussed in more detail in Sec. 4.

One of the main advantages of this technique is that for sufficiently high Q values, the sum peak forms beyond terrestrial and beam-induced backgrounds. For some reactions of interest, the sum peak forms between 8–12 MeV. This region is marked in the sum spectrum shown in Fig. 1. showing two-week background runs taken with HECTOR; the red line shows the rates for a background taken at the NSL (Surface) whereas the blue line shows rates for background taken underground at CASPAR. In both cases the background in the sum-peak region is much lower compared to the terrestrial background that spans up to about 2.6 MeV. However, on the surface there is significant background in the sum-peak region due to cosmic muons which ultimately limits HECTOR's ability to measure low cross sections. However, as can be seen in Fig. 1 the cosmic-ray induced background is greatly reduced when HECTOR is taken underground to CASPAR. With the reduction of the cosmic-muon background, other features become distinctly visible such as internal contamination of the crystals by U, Th, and daughter nuclei between 4–6 MeV, as well as a pronounced peak at 6.8 MeV stemming from neutron capture onto the crystals. The structure of the background is comparable to what has been observed by other NaI detectors at underground labs [11]. The difference in background rates between surface and underground measurements for the expected sum-peak region is over four orders of magnitude. At these rates it is estimated that HECTOR can measure cross sections below a nanobarn, making it a prime candidate to be used in the measurements of the aforementioned stellar-burning nucleosynthesis reactions.

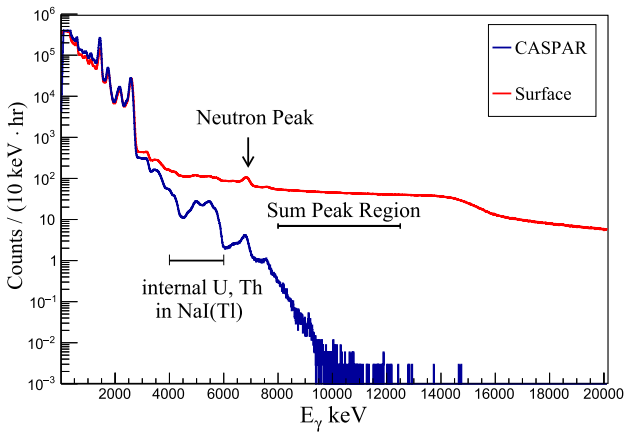

Fig. 1 Background rates for sum spectra taken with HECTOR at surface level (red) and 4,850 feet underground at CASPAR (blue). Rates were calculated using two-week background measurements

In this work we present the in-beam commissioning of HECTOR at CASPAR through the measurements of resonance strengths in the well-studied ^{27}Al$(p,\gamma)^{28}$Si reaction between lab energies 0.2–1 MeV. The 991.9, 887.8, 632.2, 405.3, and 292.6 keV-resonances were investigated. In Sect. 2 the target setup is discussed. In Sect. 3 we present the analysis details of the experiment. In Sect. 4 and 5 we present and compare two approaches in estimating the summing efficiency of the detector: one which relies on simulating the γ-ray cascades based on the known level scheme, and a statistical method that creates and simulates random γ-ray cascades for when the level scheme is not known. In Sect. 6 we present and discuss our measured resonance strengths compared to values reported in the literature.

2 Experimental Method

The measurements were performed at CASPAR using the JN 1-MV accelerator to generate protons between lab energies 0.2–1.0 MeV. The protons impinged onto a thin aluminum target corresponding to a 20 keV energy loss measured at the 405.3-keV resonance. The target was created at the NSL through the melting and evaporation of high-purity (99.99%) aluminum pellets onto a 0.5 mm thick tantalum backing.

Each resonance was scanned in 0.5–2.0 keV steps in order to identify the resonance plateau and the front edge. In addition, an off-resonance measurement was taken approximately 5–10 keV below each front edge to estimate the direct capture component of the reaction.

During experiment, data from HECTOR was processed by the NSCL Digital Data Acquisition System (DDAS) [12]. It is comprised of three XIA Pixie 16 modules [13] which are 16-channels 14-bit 100 MSPS digitizers. Two modules read the signal directly from the PMTs while the third one was used for monitoring purposes. DDAS was triggered by each individual PMT which had a discriminator threshold set just above the noise level (about 20 keV). While HECTOR has the ability to use an external trigger (see [7] for more details), it was not used in this commissioning experiment.

The target setup was modified from that of [7] to accommodate much higher beam intensities required for measurements at CASPAR. In Fig. 2 a model of the setup can be seen. Only half of the array is shown and the beam pipe has been made transparent so the internal components can be seen. The aluminum target was encased in an aluminum target holder which attached to the end of the beam pipe located at the center of HECTOR. The target was cooled using deionized water provided through nylon hoses fed into the back of the target. In order to prevent carbon buildup on the target, a cold

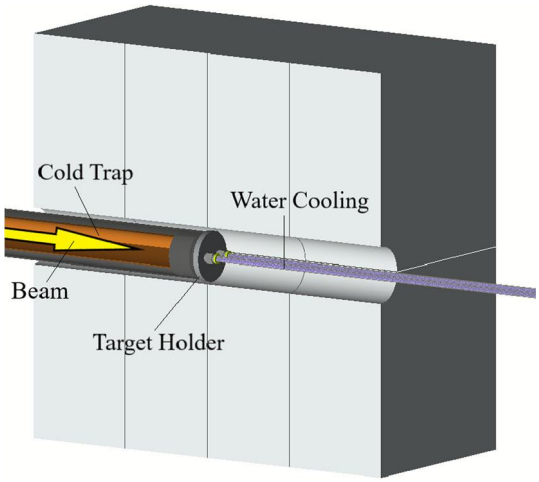

Fig. 2 A visualization of the Geant4 construction of the HECTOR target setup. Only half of the array is shown and the beam pipe is transparent to show internal components

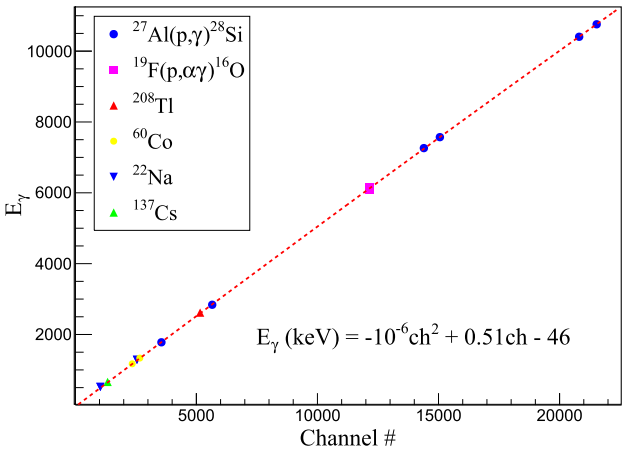

Fig. 3 Energy calibration for one of the 16 segments of HECTOR

trap was used in which a liquid-nitrogen cooled copper tube was installed 2 mm in front of the target. In addition, the cold trap was biased with a -300 V voltage to suppress secondary electron collection on to it.

The total number of particles incident on the target was determined by electrically isolating the target holder and beam pipe from the detector and ground, effectively turning them into a single Faraday cup. Thus, the deposited charge was collected and integrated using a current digitizer. The beam current was varied between 1–20 μA depending on the strength of the resonance being scanned in order to minimize pileup. Throughout the experiment the total detector dead time was kept below 1%.

3 Analysis

Before the experiment, each PMT of HECTOR was gain matched using a ^{60}Co calibration source. The calibration source was also used after the experiment to verify that the gain did not significantly change throughout the experiment. A unique energy calibration was performed for each of the 16 segments of HECTOR. The calibration utilized several calibration sources (eg., ^{22}Na, ^{137}Cs, and ^{60}Co) as well as γ rays from the resonances of the ^{27}Al$(p,\gamma)^{28}$Si reaction. Figure 3 shows an energy calibration for one of the inner segments of HECTOR. While the calibration appears linear, a second-order polynomial is used to correct for slight non-linearities observed for γ-ray energies above 10 MeV.

Each resonance analyzed in this work are sufficiently narrow such that the de Broglie wavelength of the incident particles, reaction widths, and stopping energy can be treated as constants over the resonances. Furthermore, the total energy loss of the impinged protons through the target is much greater than the width of each resonance such that the target can be treated as essentially an infinitely thick target. Under these conditions the resonance strength $\omega\gamma$ of each resonance can then be calculated from the infinitely-thick target formula [14]:

$$\omega\gamma = \frac{N_\Sigma}{N_p\,\varepsilon_\Sigma}\frac{2}{\lambda_r^2}\left(\frac{M_t}{M_t+m_p}\right)T(E_p), \tag{1}$$

where N_Σ is the number of counts in the sum peak, N_p is the number of incident particles, ε_Σ is the summing efficiency, λ_r is the de Broglie wavelength at the resonance energy, m_p and M_t are the projectile and target masses, respectively, and $T(E_p)$ is the stopping power of the beam in the target evaluated at the resonance energy. The stopping power was calculated at each resonance energy using SRIM software [15]. A 5% uncertainty was assumed for each stopping power value.

The procedure for extracting the yield for each resonance is as follows. For each run identified on the resonance plateau, the off-resonance was scaled by the ratio of N_p for the on- and off-resonance runs and subtracted from the on-resonance spectrum to remove the direct capture contribution. An on-resonance run, off-resonance run, and subtracted spectrum for the 991.9-keV resonance is shown in the top panel of Fig. 4. For each resonance analyzed in this work the off-resonance contribution is negligible. The only significant source of in-beam background at higher energies appears around 6 MeV due to the decay of ^{16}O from the ^{19}F$(p,\alpha\gamma)^{16}$O reaction which is a common contaminant in proton induced measurements. However, since the Q value of ^{27}Al$(p,\alpha\gamma)^{28}$Si is 11.6 MeV, the sum peak forms well beyond the 6 MeV region and is therefore not a concern.

After subtraction of the off-resonance, a five-parameter function combining a Gaussian with a first-order polynomial was fitted to the sum peak. The linear background compo-

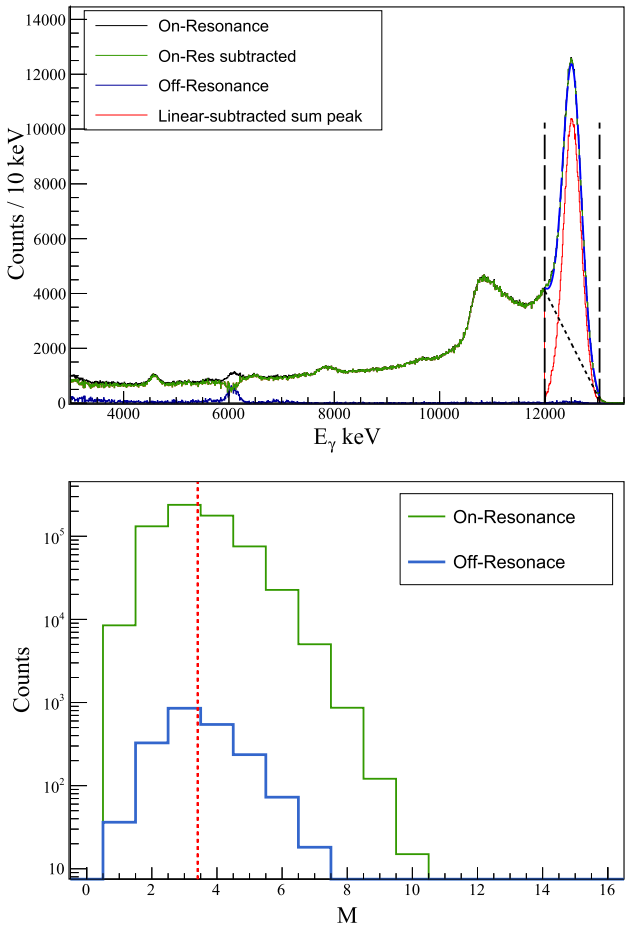

Fig. 4 Analysis of a run on the the 991.9-keV resonance plateau. Top panel: Sum spectrum showing fitting of the sum peak. Dotted black line shows the linear background to be subtracted while the dashed lines show the 3σ integration region. The red histogram is the linear-subtracted sum peak to be integrated. Bottom panel: Segment multiplicities for events corresponding to the integrated sum peak region. The dotted red line marks the mean of the distribution $\langle M \rangle$

nent, which include incomplete summation events, was then subtracted from the sum peak. The residual peak after all subtractions was then integrated within a 3σ region about the fitted mean of the sum peak. The top panel of Fig. 4 shows an example of the fitting procedure of the sum peak with the linear-subtracted residual sum peak shown in red while the integration region is marked by vertical-dashed black lines. The bottom panel of Fig. 4 shows segment multiplicities for events corresponding to the integrated sum peak region. This distribution is used to estimate the summing efficiency in the statistical approach discussed in Sect. 5.

For each run, the uncertainty of N_Σ was calculated by $\sqrt{N_T + N_{lb}}$ where N_T is the number of counts in the unsubtracted sum peak and N_{lb} is the number of counts subtracted off due to the linear background. The uncertainty of N_p was assumed to be 5% for each run. The uncertainty in the yield was calculated by the propagation of these uncertainties using standard quadrature. The total yield for the resonance, and its uncertainty, was then calculated by taking a weighted average of the yields of the runs analyzed on the resonance plateau.

4 Geant4 Simulations and Summing Efficiency using known Level Schemes

Since the first commissioning of HECTOR, the summing efficiency has been studied and analyzed through use of Geant4 [16] simulations. With the new setup at CASPAR, several components of the target holder construction have been modified along with the introduction of new components. The detector response, and subsequently the summing efficiency, depends sensitively on the amount of material present in the setup.

In order to create the most accurate simulations possible, as in the previous commissioning effort at the NSL [7], the new target setup was implemented in Geant4 and verified by comparing simulated energy spectra with those produced by calibration sources such as ^{60}Co and ^{137}Cs. Figure 5 shows a sum spectrum for a ^{60}Co source place at the center of HECTOR compared to a Geant4 simulation. The simulation is normalized to the activity of the source. Applying the fitting procedure discussed in the previous section, the integrated counts for the experimental and simulated sum peak agree within 2%.

With a proper code established, one can determine the summing efficiency of a reaction of interest by comparing the yield of the simulated sum peak to the total number of events simulated. Since the level scheme of the reaction product ^{28}Si is well known up to 13 MeV, the summing efficiency was calculated by simulating the γ-ray cascades that correspond to the transitions between the known levels with the known

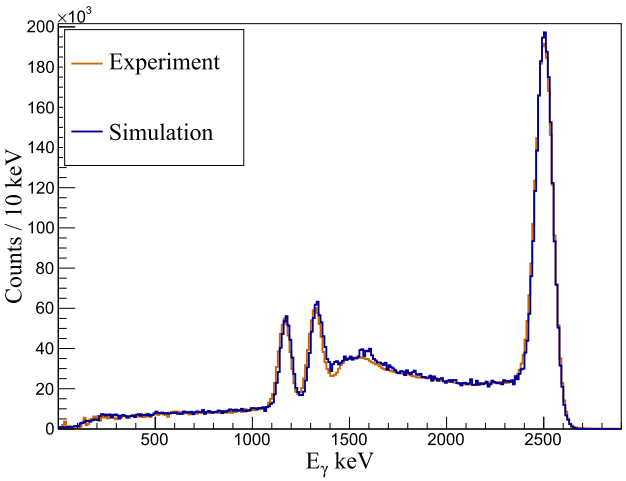

Fig. 5 Comparison of Geant4 simulations with experiment for a ^{60}Co source placed at the center of HECTOR"

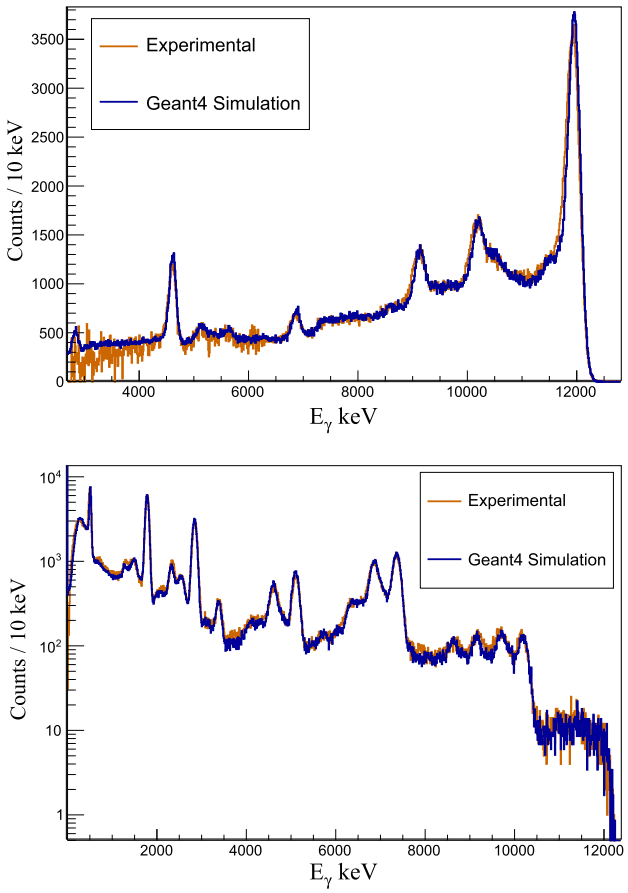

Fig. 6 Comparison of Geant4 simulations with experiment for the ^{27}Al$(p,\gamma)^{28}$Si 405.3-keV resonance. Top panel: Sum spectrum. Bottom panel: Sum-of-segments spectrum gated on sum-peak energy window

branching ratios. Branching information for primary-γ transitions for entry states into ^{28}Si was collected from various sources: For the 292.6-keV resonance, [17] was used. For the 403.3-keV resonance, [18] was used. For the 991.9-keV resonance, [19] was used. For the 632.2-keV and 887.8-keV resonances, the branching information from [20] was used. Branching information for secondary-γ transitions was collected from [21].

Figure 6 shows a comparison between experimental data and simulation of the 405.3-keV resonance. The top figure is the sum spectrum. The bottom figure shows the combined individual-segment spectra gated on the total-summed energy for an event within the 3σ integrated sum-peak region. This "sum-peak gated" spectrum, within the limit of the resolution of the detector, reflects the cascades from the entry state down to the ground state. As can be seen in both figures, there is excellent agreement between experimental and simulated spectra.

In order to calculate the summing efficiency and estimate its uncertainty, the branching ratios were modified and simulated 1000 times in a Monte Carlo approach. This was done by sampling branching ratios from a Gaussian with mean equal to the branch value and standard deviation equal to the uncertainty that was reported in the literature from which it was collected. The branching information for the 632.2 keV and 887.8-keV resonances collected from [20] does not report uncertainties on the branching ratios. Therefore for these two cases a 5% uncertainty was assumed for the dominant branching and a 20% uncertainty for the rest.

For each simulation, using the same analysis procedure, the simulated sum peaks were fitted, subtracted, and integrated to determine the summing efficiency. The summing efficiency for each resonance was then taken as the mean of the summing efficiencies from the 1000 simulations. The uncertainty was taken as the sample standard deviation of the distribution.

5 Summing Efficiency using Statistical Method

While the level scheme for ^{28}Si was sufficiently well-known for the purposes of this work, there are many cases where the branching information may be incomplete or unknown entirely. To circumvent this issue, a statistical approach for estimating the summing efficiency which requires no knowledge of the level scheme was established [7]. As this approach will be used in future works, the summing efficiency for the five resonances measured in this work have also been estimated using this statistical method. It will be shown that it is consistent with summing efficiencies calculated using the known level-scheme approach.

In the statistical approach the summing efficiency is estimated by experimentally measuring the average segment multiplicity $\langle M_{exp}\rangle$ for events corresponding to the sum peak. More precisely, $\langle M_{exp}\rangle$ is defined as the mean of the segment multiplicities for events with sum energies within the same 3σ integrated region used to determine N_Σ. This distribution is shown for the 991.9 keV case in the bottom of Fig. 4. Contributions from direct capture are considered by scaling and subtracting the multiplicities of events in the same integration region from the off-resonance run. A $\langle M_{exp}\rangle$ is determined for each run analyzed on the resonance plateau. The $\langle M_{exp}\rangle$ of the resonance is taken as the mean of these values while the uncertainty is taken as the sample standard deviation.

The next step is to create simulated sum peaks from which $\langle M\rangle$ and summing efficiencies can be calculated. Thousands of simulations were performed using a fixed sum-peak energy but varying the average number of γ rays emitted. For each simulation, the summing efficiency and $\langle M\rangle$ are extracted using the same analysis previously discussed. When the summing efficiencies are plotted as a function of $\langle M\rangle$, they create the so-called efficiency curves.

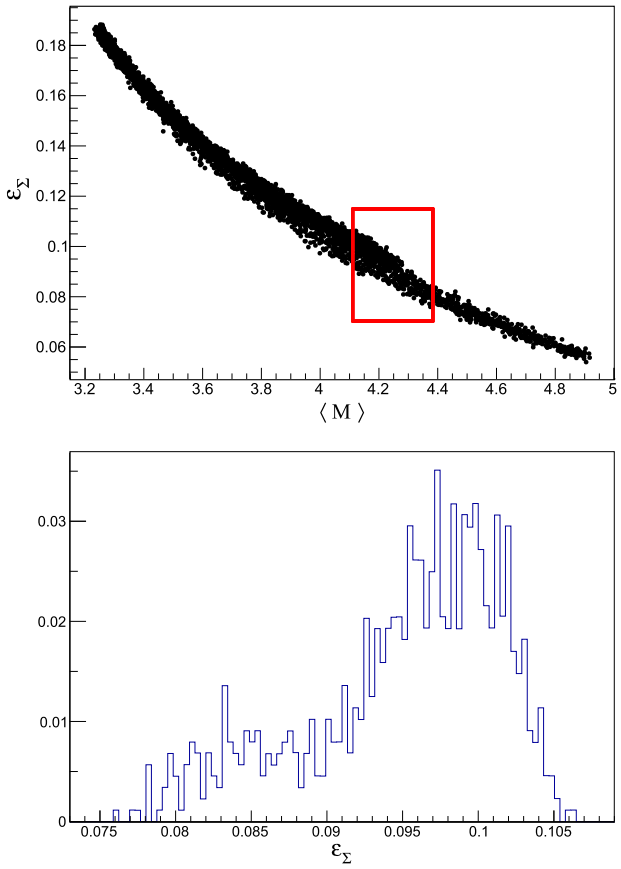

Fig. 7 Top panel: An efficiency curve for a sum peak of 11-867 keV used to analyze the 292.6-keV resonance. The red box marks the region of efficiency points near $\langle M_{exp} \rangle$ used to estimate the summing efficiency probability distribution. Bottom panel: Projection of the efficiencies within the gated region normalized with a total area equal to unity

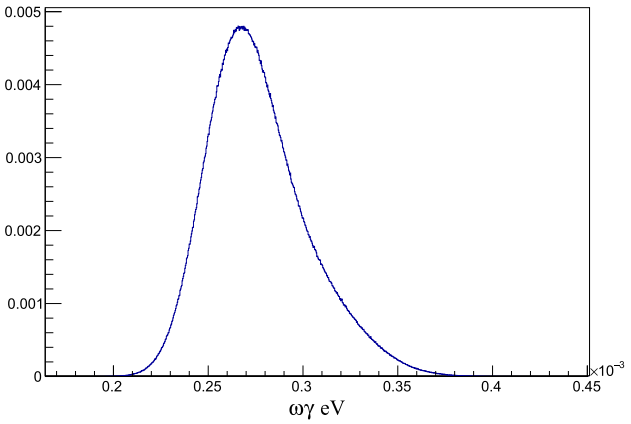

Fig. 8 A probability distribution for the 292.6-keV resonance strength calculated using Monte Carlo methods described in the statistical approach

Table 1 Average segment multiplicities $\langle M \rangle$ and summing efficiencies ε_Σ. *exp* denotes experimentally measured values. *l. s.* and *stat* are quantities calculated using the known level scheme and statistical approach respectively

E_p keV	$\langle M \rangle$ *exp*	$\langle M \rangle$ *l. s.*	ε_Σ *l. s.*	ε_Σ *stat*
292.6	4.25(5)	4.20(1)	0.0987(7)	$0.096\,^{0.009}_{0.005}$
405.3	4.18(6)	4.168(5)	0.102(1)	$0.097\,^{0.007}_{0.008}$
632.2	3.40(1)	3.38(2)	0.165(2)	0.163(2)
887.8	2.53(9)	2.45(2)	0.265(5)	0.26(3)
991.9	3.40(1)	3.373(5)	0.163(1)	0.164(2)

An efficiency curve, which was used to analyze the 292.6-keV resonance, is shown in the top figure of Fig. 7. Each point on the efficiency curve represents a single simulation where 100 different γ-ray cascades were simulated. The energies of each individual γ ray were determined by randomly sampling from a uniform distribution. However, the energies were constrained such that the sum of the γ-ray energies in each cascade equaled the sum-peak energy.

Among the thousands of simulations that were performed, only the simulations that produce a $\langle M \rangle$ similar to the measured $\langle M_{exp} \rangle$ are considered. In the case of the efficiency curve in Fig. 7, a red box centered at $\langle M_{exp} \rangle$ with a width three times the experimental uncertainty marks the efficiency points considered in the analysis. The bottom panel of Fig. 7 shows the projection of these summing efficiencies.

Because of the many different combinations of γ-ray cascades that can generate a $\langle M \rangle$ comparable to $\langle M_{exp} \rangle$, a well-defined summing efficiency cannot be determined. Rather the statistical method generates a probability distribution function (pdf) where it is assumed that the true summing efficiency is contained within this distribution. Unlike the summing efficiency distribution that was produced using the known level-scheme approach, this efficiency pdf is not assumed to be a normal distribution. Therefore, standard quadrature procedures cannot be used to propagate the uncertainty of the summing efficiency into $\omega\gamma$. Instead, a Monte Carlo method was used to create a pdf for $\omega\gamma$ by sampling values from pdfs of the yield, stopping power, and efficiency and using Eq. 1. The yield and stopping power were sampled as Gaussians with means equal to their measured values and standard deviations equal to their uncertainties.

The pdf for the 292.6 keV $\omega\gamma$ is shown in Fig 8. It is nearly Gaussian, but the distribution is slightly skewed due to the convolution of the asymmetrical summing efficiency pdf which is shown in the bottom panel of Fig. 7. From the pdf of $\omega\gamma$ we report the median of the distribution while the lower and upper errors are reported as the the 16^{th} and 84^{th} percentiles of the distribution, respectively.

Summing efficiencies calculated from both approaches are shown in Table 1. The summing efficiencies estimated from the statistical approach are in remarkably good agreement with those calculated using the known level schemes. For all

Table 2 Resonance strengths $\omega\gamma$ for the ^{27}Al(p, γ)^{28}Si reaction measured in this work compared with values from the literature. *l. s.* are $\omega\gamma$ calculated using known level schemes and *stat* are $\omega\gamma$ estimated using the statistical approach

E_p keV	This Work (*l.s.*)	This Work (*stat*)	NACRE [22]	Others (refs. given in brackets at end of corresponding $\omega\gamma$)
	$\omega\gamma$ eV			
292.6	$2.65(17) \times 10^{-4}$	$2.73\,^{0.29}_{0.22} \times 10^{-4}$	$3.8(7) \times 10^{-4}$	$2.67^{b} \times 10^{-4}$ [23], $2.80(15) \times 10^{-4}$ [24]
405.3	$9.76(51) \times 10^{-3}$	$10.3\,^{0.7}_{0.6} \times 10^{-3}$	$9.0(10) \times 10^{-3}$	$1.0(2) \times 10^{-2}$ [25], $8.63(52) \times 10^{-3}$ [18], $1.04(5) \times 10^{-2}$ [24]
632.2	0.266(13)	0.269(14)	0.266(14)	0.25(3) [25], 0.267(25) [26], .268(18) [27], 0.217(43) [28], 0.29(3) [24]
887.8	$1.22(7) \times 10^{-2}$	$1.24\,^{0.19}_{0.15} \times 10^{-2}$	$1.5(2) \times 10^{-2}$	$1.33(25) \times 10^{-2}$ [25], $1.20(15) \times 10^{-2}$ [24]
991.9	1.94(10)	1.93(10)	1.9(1)	1.83(20) [25], 1.95(15)[a], 1.93(13) [27], 2.00(17) [23], 2.00(15) [24]

[a] Calculated using yield from [29]
[b] No uncertainty reported for this work

five resonances, the summing efficiencies calculated using known level schemes are contained with a 95% confidence interval estimated by the statistical approach. Therefore the resonance strengths calculated from both approaches are in good agreement. However, we recommend adopting the resonance strengths calculated from the known level schemes due to the excellent agreement seen between simulation and experiment. The agreement in resonances strengths between both methods shows that the statistical method can be used in cases where the level schemes are not known.

It is worth noting that the ability of the statistical method to produce a distribution of efficiencies with low relative error on the order of 5–10% was achieved by imposing constraints on the simulated cascades that created the efficiency curves. This was done to best reflect properties of true cascades in ^{28}Si. In particular, this was done by limiting cascades to no more than four γ rays emitted as analysis of the known level schemes showed that cascades with five or more γ rays emitted make up less than 1% of the total cascades. Furthermore, for all the resonances except the 887.8 keV, single γ ray transitions directly from entry to ground were omitted as the γ_0 contribution for those resonances are negligible. As a final constraint, the energy of every γ ray in simulation was at least 500 keV, again reflecting the fact that no low-energy γ rays were observed in the level scheme.

In general, when there is less information about the residual nuclei more variations and cases for the simulated cascades will need to be considered. The combination of these variations can be still be combined into a single efficiency pdf. This will minimize possible systematic uncertainties or bias in the efficiency curves. However, including more variations will naturally produce a broader efficiency distribution and the relative error will increase.

6 Results and Discussion

Resonance strengths calculated using summing efficiencies from the known level scheme and statistical approach are listed in Table 2. They are labeled under *l.s.* and *stat* respectively. Again we recommend adopting the *l.s.* values as they are more precise measurements on the order of 5%. Also listed in Table 2 are resonance strengths listed in the NACRE compilation [22] as well as various other measurements found in the literature.

Comparing our measurements to those in the literature, in general there is good agreement seen across all five resonances investigated. For the well-known 991.9-keV and 632.2-keV resonances, there is excellent agreement with two independent measurements [27] and [29] which have similar precision on the order of 7%. In [29], only a thick-target yield of the 1778.9 -keV γ ray is reported, so we have calculated the resonance strength shown in Table 2 using the same stopping power used in this work and assuming a branching ratio for the 1778.9 keV line of 94.8(15) [19]. For the 405.3-keV resonance, our measurement falls in between [18] and [24] which is in good agreement when the uncertainties in the measurements are considered. For the lesser known 292.6 keV and 887.8-keV resonances there is excellent agreement seen with [24] where the γ-summing technique was also employed.

7 Summary

In order to measure cross sections of stellar nucleosynthesis reactions in the physically relevant energy ranges, HECTOR has recently been commissioned 4,850 feet underground at CASPAR. The underground shielding from cosmic rays drastically reduces the background rates where the sum peak is expected to form. This will allow cross section measurements with HECTOR to be pushed below the nanobarn range. An in-beam commissioning experiment for the target setup at CASPAR was performed where several resonance strengths in the ^{27}Al(p, γ)^{28}Si reaction were measured for lab energies between 0.2 and 1.0 MeV. The resonance strengths were calculated using summing efficiencies from two different approaches: one using the known level schemes, and a statistical method that was developed for when the level scheme is not known. The resonance strengths calculated from both approaches are in good agreement with one another and are in excellent agreement with values from the literature.

Acknowledgements This work was supported by the National Science Foundation (NSF) under Grants nos. PHY-1713857, PHY-2011890, PHY-1614442, and PHY-1913746, and the Sanford Underground Research Facility (SURF) under Award number DE-SC0020216.

Data Availability Statement This manuscript has no associated data or the data will not be deposited. [Authors' comment: Results relevant to the discussion in the paper are included in appropriate figures and tables within the text. All experimental data is available upon request to the corresponding author.]

References

1. M. Wiescher, F. Käppeler, K. Langanke, Annu. Rev. Astron. Astrophys. **50**(1), 165 (2012). https://doi.org/10.1146/annurev-astro-081811-125543
2. D. Bemmerer, F. Confortola, A. Lemut, R. Bonetti, C. Broggini, P. Corvisiero, H. Costantini, J. Cruz, A. Formicola, Z.S. Fülöp et al., Eur. Phys. J. A **24**(2), 313 (2005). https://doi.org/10.1140/epja/i2004-10135-4
3. W. Liu, Z. Li, J. He et al., Sci. China Phys. Mech. Astron. **59**, 642001 (2016). https://doi.org/10.1007/s11433-016-5785-9
4. T. Szücs, D. Bemmerer, D. Degering et al., Eur. Phys. J. A **55**, 174 (2019). https://doi.org/10.1140/epja/i2019-12865-4
5. D. Robertson, M. Couder, U. Greife, F. Strieder, M. Wiescher, EPJ Web Conf. **109**, 09002 (2016). https://doi.org/10.1051/epjconf/201610909002
6. StGobain Crystals (2016)
7. C.S. Reingold, O. Olivas-Gomez, A. Simon, J. Arroyo, M. Chamberlain, J. Wurzer, A. Spyrou, F. Naqvi, A.C. Dombos, A. Palmisano et al., Eur. Phys. J. A **55**(5), 77 (2019). https://doi.org/10.1140/epja/i2019-12748-8
8. O. Olivas-Gomez, A. Simon, O. Gorton, J.E. Escher, E. Churchman, P. Millican, R. Kelmar, C.S. Reingold, A.M. Clark, N. Cooper et al., Phys. Rev. C **102**, 055806 (2020). https://doi.org/10.1103/PhysRevC.102.055806
9. R. Kelmar, A. Simon, O. Olivas-Gomez, P. Millican, C.S. Reingold, E. Churchman, A.M. Clark, S.L. Henderson, S.E. Kelly, D. Robertson et al., Phys. Rev. C **101**, 015801 (2020). https://doi.org/10.1103/PhysRevC.101.015801
10. A. Spyrou, H.W. Becker, A. Lagoyannis, S. Harissopulos, C. Rolfs, Phys. Rev. C **76**, 015802 (2007). https://doi.org/10.1103/PhysRevC.76.015802
11. H. Ohsumi, R. Gurriarán, P. Hubert, R. Arnold, C. Augier, J. Baker, A. Barabash, O. Bing, V. Brudanin, A. Caffrey et al., Nucl. Instrum. Methods Phys. Res. Sect. A Accel. Spectrom. Detect. Assoc. Equip. **482**(3), 832 (2002). https://doi.org/10.1016/S0168-9002(01)01866-6
12. C. Prokop, S. Liddick, B. Abromeit, A. Chemey, N. Larsen, S. Suchyta, J. Tompkins, Nucl. Instrum. Methods A **741**, 163 (2014)
13. XIA LLC. http://www.xia.com/DGF_Pixie-16.html (2016)
14. C. Iliadis, *Nuclear Physics of Stars* (Wiley, New York, 2018), pp. 345–348. https://doi.org/10.1002/9783527692668.ch4
15. J.F. Ziegler, M.D. Ziegler, J.P. Biersack, Nucl. Instrum. Methods Phys. Res. B **268**(11–12), 1818 (2010). https://doi.org/10.1016/j.nimb.2010.02.091
16. J. Allison, K. Amako, J. Apostolakis, P. Arce, M. Asai, T. Aso, E. Bagli, A. Bagulya, S. Banerjee, G. Barrand et al., Nucl. Instrum. Methods Phys. Res. Sect. A Accel. Spectrom. Detect. Assoc. Equip. **835**, 186 (2016). https://doi.org/10.1016/j.nima.2016.06.125
17. C. Iliadis, T. Schange, C. Rolfs, U. Schroeder, E. Somorjai, H. Trautvetter, K. Wolke, P. Endt, S. Kikstra, A. Champagne et al., Nucl. Phys. A **512**, 509 (1990)
18. D. Powell, C. Iliadis, A. Champagne, S. Hale, V. Hansper, R. Surman, K. Veal, Nucl. Phys. A **644**(4), 263 (1998). https://doi.org/10.1016/S0375-9474(98)00593-4
19. A. Antilla, J. Keinonen, M. Hautala, I. Forsblom, Nucl. Instrum. Methods **147**(3), 501 (1977). https://doi.org/10.1016/0029-554X(77)90393-7
20. M. Meyer, I. Venter, D. Reitmann, Nucl. Phys. A **250**(2), 235 (1975). https://doi.org/10.1016/0375-9474(75)90256-0
21. National Nuclear Data Center. https://www.nndc.bnl.gov/ (2021)
22. C. Angulo, M. Arnould, M. Rayet, P. Descouvemont, D. Baye, C. Leclercq-Willain, A. Coc, S. Barhoumi, P. Aguer, C. Rolfs et al., Nucl. Phys. A **656**(1), 3 (1999). https://doi.org/10.1016/S0375-9474(99)00030-5
23. P.M. Endt, Nucl. Phys. A **633**, 1 (1998)
24. S. Harissopulos, K.S.C. Chronidou, T. Paradellis, C. Rolfs, W. Schulte, H. Becker, Eur. Phys. J. A **9**, 479 (2000)
25. P. Lyons, J. Toevs, D. Sargood, Nucl. Phys. A **130**(1), 1 (1969). https://doi.org/10.1016/0375-9474(69)90954-3
26. J. Keinonen, M. Riihonen, A. Anttila, Physica Scripta **12**(5), 280 (1975). https://doi.org/10.1088/0031-8949/12/5/005
27. B. Paine, D. Sargood, Nucl. Phys. A **331**(2), 389 (1979). https://doi.org/10.1016/0375-9474(79)90349-X
28. J. Brenneisen, D. Grathwohl, M. Lickert, R. Ott, R. Höpke, J. Schmälzlin, B. Wildenthal, Z. Phys. A **352**, 149 (1995)
29. J. Keinonen, A. Anttila, Commentationes Physico-Mathematicae **46**, 61 (1976)